



## SUBJECT AREAS:

MOLECULAR  
NEUROSCIENCE  
BEHAVIOUR  
PLASTICITY  
NEUROGENETICS

# The hematopoietic cytokine granulocyte-macrophage colony stimulating factor is important for cognitive functions

Markus Krieger<sup>1</sup>, Martin Both<sup>2</sup>, Simon A. Kranig<sup>2</sup>, Claudia Pitzer<sup>1</sup>, Matthias Klugmann<sup>3</sup>, Gerhard Vogt<sup>1</sup>, Andreas Draguhn<sup>2</sup> & Armin Schneider<sup>1</sup><sup>1</sup>SYGNIS Bioscience, Im Neuenheimer Feld 515, 69120 Heidelberg, Germany, <sup>2</sup>Institute for Physiology, University of Heidelberg, Im Neuenheimer Feld 346, 69120 Heidelberg, Germany, <sup>3</sup>Translational Neuroscience Facility, Department of Physiology, School of Medical Sciences, University of New South Wales, UNSW Kensington Campus, Sydney, NSW, 2052, Australia.Received  
17 July 2012Accepted  
12 September 2012Published  
26 September 2012Correspondence and  
requests for materials  
should be addressed to  
A.S. (Schneider@  
Sygnis.de)

We recently reported expression of hematopoietic growth factor GM-CSF and its receptor (GM-CSFR) in CNS neurons. Here we evaluated this system in learning and memory formation using GM-CSF deficient mice. In complementation, GM-CSF signalling was manipulated specifically in adult murine hippocampus by adeno-associated virus (AAV)-mediated GM-CSFR alpha overexpression or knock-down. GM-CSF ablation caused various hippocampus and amygdala-dependent deficits in spatial and fear memory while rendering intact basic parameters like motor function, inherent anxiety, and pain threshold levels. Corroborating these data, spatial memory of AAV-injected mice was positively correlated with GM-CSFR $\alpha$  expression levels. Hippocampal neurons of knock-out mice showed markedly pruned dendritic trees, reduced spine densities, and lower percentages of mature spines. Despite such morphological alterations, long-term potentiation (LTP) was unimpaired in the knock-out hippocampus. Collectively, these results suggest that GM-CSF signalling plays a major role in structural plasticity relevant to learning and memory.

Granulocyte-macrophage colony stimulating factor (GM-CSF) was originally identified as a hematopoietic growth factor that regulates the generation and functional activation of myeloid lineage cells<sup>1,2</sup>. This secreted glycoprotein exerts its functions by binding to heteromeric cell-surface receptors composed of  $\alpha$  subunits (GM-CSFR $\alpha$ ) that confer ligand specificity and  $\beta$  subunits ( $\beta_c$ ) shared with receptors for interleukin (IL)-3 and IL-5 that mediate intracellular signalling<sup>3</sup>. Clinically, GM-CSF is in use for the treatment of chemotherapy-associated neutropenia and is regarded as a well-tolerated protein<sup>4,5</sup>. It has also been evaluated for use in inflammatory bowel disease<sup>6</sup>.

We have recently found constitutive neuronal GM-CSFR $\alpha$  expression in many regions of the adult rodent brain, as well as enhanced GM-CSF and GM-CSFR $\alpha$  expression levels in a cortical stroke model<sup>7</sup>. In neurons, GM-CSF activates the PI3K/Akt, stat3, Erk1/2, and Erk5 signalling pathways, and induction of PI3K/Akt appears mainly responsible for the potent anti-apoptotic functions of neuronal GM-CSF signalling<sup>7</sup>. Prominent neuro-protective effects were found for GM-CSF in animal models for stroke<sup>7-9</sup> and Parkinson's disease<sup>10</sup>. Additionally, GM-CSF exerts pro-neurogenic effects on adult neural stem cells<sup>11</sup>. The GM-CSF receptor has also been identified on paraventricular and arcuate nucleus neurons, where it appears involved in food intake regulation<sup>12</sup>. Together, these findings confirm GM-CSF as a neuronally active growth factor. Similar functions have been described for the two other major hematopoietic proteins granulocyte colony stimulating factor (G-CSF) and erythropoietin (EPO), defining these three proteins as a novel class of neurotrophic growth factors<sup>13</sup>. Importantly, systemically applied GM-CSF crosses the blood-brain barrier<sup>14</sup>, thus rendering GM-CSF a potentially promising pharmacological approach for the treatment of CNS dysfunctions.

Pro-cognitive effects have been well established for a number of growth factors, the most well-known being brain derived neurotrophic factor (BDNF) and nerve growth factor<sup>15,16</sup>. As GM-CSFR $\alpha$  is expressed on neurons in regions associated with learning and memory such as the cortex and hippocampus<sup>7</sup>, we asked whether GM-CSF may be similarly involved in aspects of cognition. To address this question, we systematically tested GM-CSF deficient (GMko) mice<sup>17</sup> in a battery of behavioural paradigms that assessed learning and memory formation as

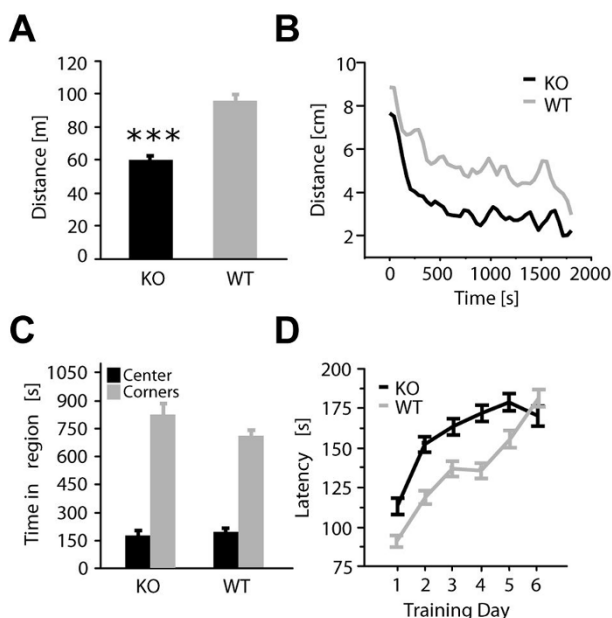


**Figure 1 | Spontaneous and forced locomotion, anxiety, and exploration.** (A) Spontaneous locomotor activity in the open field was reduced in GMko mice which travelled shorter overall distances over the course of a 30 min testing period (genotype,  $p < 0.001$ ). (B) Open-field activity was consistently lower in GMko mice (genotype,  $p < 0.001$ ) and no initial anxiety-related immobility or altered habituation rate (genotype\*time,  $p > 0.05$ ) was noted. (C) Times spent in the corner or center regions of the arena were similar between groups (both  $p > 0.05$ ). (D) Compared to controls, forced motor activity was improved in GMko mice (genotype,  $p < 0.05$ ), but motor learning was impaired (genotype\*test day,  $p < 0.01$ ). WT,  $n = 18$ ; KO,  $n = 16$  animals. Data is presented as mean  $\pm$  SEM.

well as sensomotoric aspects of rodent behaviour. Morphology of dentate gyrus and CA1 neurons was analyzed to determine the impact of GM-CSF deficiency on neuronal complexity, dendritic spine counts, and spine maturation. Moreover, induction of long-term potentiation at Schaffer collaterals was examined in GMko mice. In a complementary approach, we examined spatial memory formation after specifically altering hippocampal GM-CSFR $\alpha$  levels in adult wildtypes using adeno-associated virus (AAV) vectors.

Here, we report that GM-CSF signalling in the CNS is critical for proper memory formation.

## Results

**Effects of GM-CSF deficiency on exploration, motor performance, and anxiety-related behaviour.** GMko mice showed reduced

locomotor activity levels in the open field throughout the 30 min testing period (Figure 1 A,B). This effect was not related to elevated levels of anxiety as judged by the time spent in the corner and center regions of the arena (Figure 1 C). Reduced locomotor activity was confirmed over nocturnal 12 hour periods during the animals' active phase using an automated detection system (wt,  $n = 18$ ; ko,  $n = 16$  animals). Here, GMko mice spent less time with horizontal locomotion (wt,  $3108 \pm 120$  s; ko,  $1263 \pm 128$  s;  $p < 0.001$ ) and cage climbing (wt,  $4330 \pm 411$  s; ko,  $1579 \pm 436$  s;  $p < 0.001$ ), travelled a shorter overall distance (wt,  $163.9 \pm 7.6$  m; ko,  $63 \pm 8.0$  m;  $p < 0.001$ ), and spent more time in an immobile state (wt,  $7087 \pm 750$  s; ko,  $18872 \pm 795$  s;  $p < 0.001$ ). These effects were not due to impairments of the motor system as GM-CSF deficiency did not impair but rather improve overall rotarod performance (Figure 1 D). As weight differences between the genotypes<sup>12</sup> might potentially influence rotarod performance, data was statistically analyzed in a multivariate model incorporating genotype, weight, and test day as main factors with animal identity as random effect. Test day was modelled by knotted splines to better account for deviations from linearity of rotarod performance over time. This analysis revealed a significant influence of genotype ( $p < 0.05$ ) and test day ( $p < 0.001$ ), but not of weight ( $p > 0.05$ ). There was no genotype\*weight interaction ( $p > 0.05$ ). Heightened anxiety levels were fully excluded by the dark-light box paradigm which revealed comparable anxiety levels between GMko and wildtype mice (time in light: wt,  $96.5 \pm 9.2$  s; ko,  $92.5 \pm 9.8$  s;  $p > 0.05$ ). Instead, diminished rearing behaviour in the lit compartment suggested that decreased voluntary activity in knock-outs is caused by reduced exploratory drive (rearing: wt,  $17.1 \pm 1.7$ ; ko,  $5.3 \pm 1.8$ ;  $p < 0.001$ ).

**Effects of GM-CSF deficiency on cognition.** During active place avoidance training, both groups learned to avoid the shock sector (Figure 2 A) and increased entry latencies over trials (Figure 2 B). However, acquisition was inferior and reached an early plateau in GMko mice (Figure 2 B; genotype:  $p < 0.05$ ; trial\*genotype  $p = 0.001$ ). Importantly, early occurrence of asymptotic performance levels was unlikely caused by a physical inability to master this task, given the absence of profound motor deficits in the rotarod test and the platform's slow rotational velocity of 1 rpm. Memory retention after 24 hours was likewise inferior in these animals (Figure 2C,  $p < 0.05$ ). Importantly, these observations were not due to altered plantar pain threshold levels as judged by the Hargreaves method (paw withdrawal latency: wt,  $6.4 \pm 0.3$  s; ko  $6.1 \pm 0.4$  s;  $p > 0.05$ ).

We subsequently tested animals in the Morris water maze (MWM). A visible platform version revealed no between-group differences of escape latency, path length, and velocity (data not shown). Over 12 training days (D1–D12), both groups learned the location of the hidden platform as monitored by decreasing escape latencies and path lengths (Figure 3 A,B; both  $p < 0.001$ ). In both acquisition curves, we noted considerable offset differences between groups

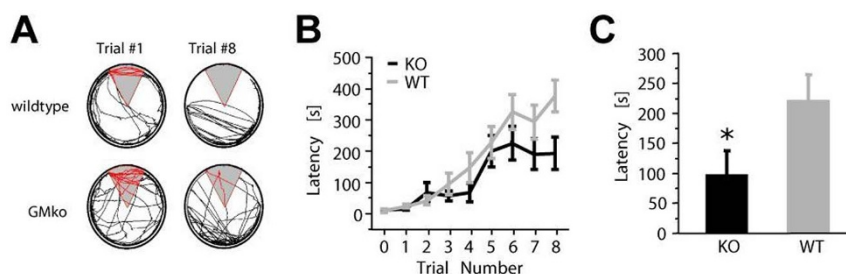


**Figure 2 | Effects of GM-CSF deficiency on spatial learning and memory in an active place avoidance paradigm.** (A) Representative trajectories of both the first and last training trials illustrating inferior learning performance of knock-out mice. (B) During acquisition, entry latencies into the shock zone were dependent on genotype with reduced place avoidance observed in GMko mice (genotype,  $p < 0.05$ ; genotype\*trial,  $p = 0.010$ ). Note the failure to further improve performance after trial 5 in these mice. (C) Shock zone entry latencies were reduced during memory recall 24 hours after training. (\*,  $p < 0.05$ ). WT,  $n = 22$ ; KO,  $n = 21$  animals. Data is presented as mean  $\pm$  SEM.

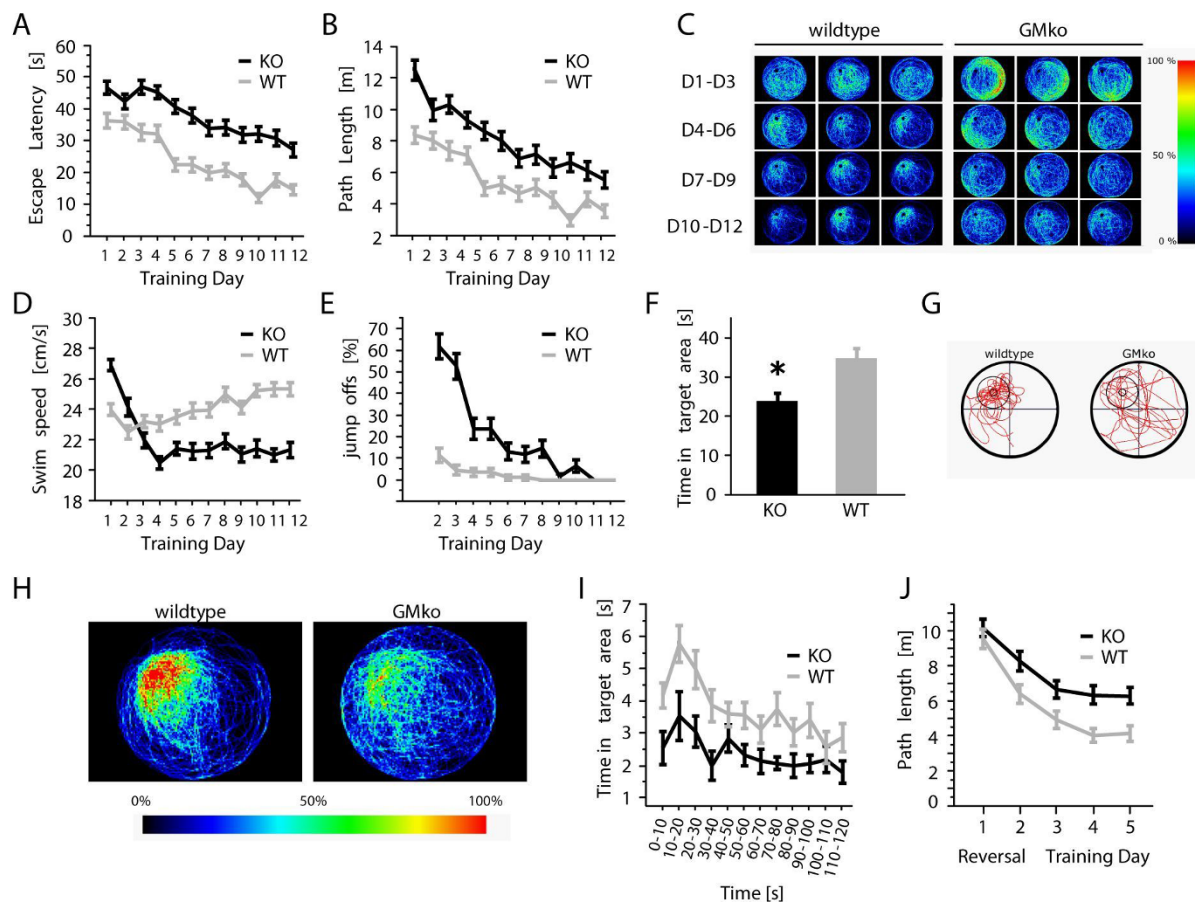


**Figure 3 | Effects of GM-CSF deficiency on MWM performance.** (A,B) During acquisition, a main effect of genotype was noted as escape latencies (A) and swim path lengths (B) were greater in GMko mice compared to controls (genotype,  $p < 0.001$ ). However, learning progress between groups was comparable as reflected by a similar relative improvement over time for both parameters (genotype\*day, both  $p > 0.05$ ). (C) Frequency density analysis of accumulated trajectories reveals thigmotactic behaviour of knock-outs during early training with an initial focus on pool entry sites. Platform-focused trajectories develop later and to a lesser extent compared to wildtypes. (D) Velocity profiles during training differed between groups (genotype,  $p < 0.01$ , genotype\*day,  $p < 0.001$ ). In contrast to controls, knock-outs displayed signs of an elevated stress response with initial hyper- and subsequent hypoactivity. (E) Only knock-outs displayed pronounced platform jump-off behaviour (genotype,  $p < 0.001$ ). This only subsided towards the end of the acquisition period. (F) Spatial memory was impaired in GMko mice which spent significantly less time in the target area during the probe trial ( $p < 0.05$ ). While performance at D12 clearly affected this parameter ( $p < 0.01$ ), genotype had an independent effect ( $p < 0.05$ ). (G) Representative probe trial trajectories illustrating reduced memory accuracy in GMko mice in the probe trial. (H) Frequency density maps illustrating inferior memory performance of GMko mice in the probe trial. (I) Occupancy of target area locations during the probe trial analyzed in bins of 10 seconds indicates differential platform search patterns between groups (genotype,  $p = 0.010$ ; genotype\*time,  $p < 0.05$ ). Controls initially perform a focused search at the former platform location (FPL) before screening other regions, while, at an overall lower rate, knock-outs keep constantly visiting the FPL. (J) Reversal learning was impaired in GMko mice (both genotype and genotype\*time,  $p < 0.05$ ). Note that path lengths were indistinguishable at reversal training day 1. WT,  $n = 22$ ; KO,  $n = 21$  animals. Data is presented as mean  $\pm$  SEM.

( $p < 0.001$ ) that were already present in the first trial ( $p < 0.05$ ), but no significant slope differences between curves (genotype\*day;  $p > 0.05$ ). Frequency density maps of swim paths revealed that GMko mice were likely found near pool entry sites during early training and needed longer to develop goal-directed behaviour with search patterns in closer vicinity to the platform (Figure 3 C). While these differential characteristics in trajectories provide a straightforward explanation for the between-group offset differences in learning curves, they also suggest that increased stress susceptibility may interfere with efficient development of search strategies in knock-out animals. In line with this, GMko mice displayed other erratic behaviours like high initial velocity (Figure 3 D,  $p < 0.001$ ) and platform jump-offs (Figure 3 E,  $p < 0.001$ ). However, we did not observe any floating behaviour, indicating absence of learned helplessness or behavioural despair as a consequence of reduced escape success in knock-outs.

The probe trial at D13 revealed a significant difference in the time spent in the target area defined as a circle ( $r = 20$  cm) around the former platform center (Figure 3 F,  $p < 0.05$ ). Covariate analysis using genotype and path length at D12 and their interaction as factors revealed an influence of genotype on recall performance ( $p < 0.05$ ) that was independent of D12 path length. Therefore, GM-CSF deficiency results in impaired spatial memory storage or recall 24 h after acquisition. Representative probe trial trajectories for both groups are shown (Figure 3 G), as well as density maps of probe trial swim paths (Figure 3 H).

To investigate potential differences in platform search strategies during the probe trial, we next analysed time spent in the target area in bins of 10 seconds. Apart from an overall offset difference (genotype  $p < 0.01$ ), the curve slopes were significantly different ( $p < 0.05$ ), suggesting differential strategies between groups. In contrast to controls, knock-outs failed to perform initially focused searches in the



target area and did not reduce their visiting time markedly upon failure to find a platform (Figure 3 I).

As this indicated diminished flexibility to adapt to new conditions, we consequently explored reversal learning where pre-trained animals were subjected to a 5-day (RD1-RD5) protocol with the platform moved from the NW to SE quadrant. As shown in Figure 3 J, reversal learning of GMko mice was clearly inferior ( $p < 0.05$ ). Collectively, these results show that GM-CSF deficiency causes profound spatial memory impairments and affects the behavioural flexibility to respond to altered environmental conditions.

To determine whether GM-CSF deficiency also impacted on fear memory formation, we tested animals on a delayed fear conditioning protocol that distinguishes between hippocampus-dependent contextual and amygdala-dependent cue-related fear memory. All animals startled in response to sudden noise generated by flicking of a rubber glove invisible to the animals, indicating absence of gross hearing deficits in both genotypes. Both groups showed equal freezing behaviour in response to repetitive cue-shock pairings during conditioning (Figure 4 A), but knock-outs showed a hippocampus-dependent contextual fear memory deficit upon challenge with the conditioning chamber 24 hours after training in the first two minutes of context exposure (Figure 4 B,  $p < 0.001$  for both first and second minute). The expected decline in freezing over time after this initial exposure was less evident for knock-outs, potentially indicative of a deficit in extinction of the context association. Moreover, when cue-related fear memory was assessed by challenge with the conditioning cue 48 hours after training, fear responses were likewise strongly reduced in GMko mice (Figure 4 C,  $p < 0.001$ ) indicating an additional impairment of amygdala-dependent fear memory. Temporal analysis of freezing behaviour confirmed the

overall difference to be due to different levels of fear responses to cue presentations (Figure 4 D).

**Effects of GM-CSF deficiency on hippocampal morphology.** Initial *in vitro* experiments indicated a stimulatory effect for GM-CSF on neurite outgrowth of primary hippocampal neurons when measuring total neurite length 48 h after stimulation with 20 ng/ml GM-CSF (GM-CSF,  $87.2 \pm 3.2 \mu\text{m}$ ; untreated,  $77.1 \pm 3.2 \mu\text{m}$ ;  $n = 100$  cells per group;  $p < 0.05$ ). We therefore investigated whether GM-CSF deficiency led to morphological deficits in GMko mice. Gross hippocampal anatomy was normal including hippocampal volume, maximal hippocampal width, and distance between dorsal tips of CA1 and DG layers of nuclei (data not shown). Nevertheless, measures of other distances between characteristic points within various planes along the rostro-caudal axis indicated minor alterations of unclear relevance in hippocampal anatomy including a slightly increased distance between CA1 and CA4 ends of the CA region in medial sections, a slightly compressed appearance of the DG with reductions in gap width between the ends of upper and lower blade of the granule cell layers, and altered distances between the CA1 end of the CA region and the junction of the upper and lower blades of the DG (Figure 5).

At the cellular level, full reconstruction of DG neurons from GMko mice ( $n = 17$  cells) and wildtypes ( $n = 19$  cells) revealed a 33% shortening of total dendritic length and a 30% decrease in dendritic bifurcations in GMko brains (Figure 6 A–C). In addition, density of dendritic spines was reduced by 15% and 31% in the DG and CA1 subfields, respectively (Figure 6 D–F). Moreover, relatively fewer dendritic spines displayed mushroom-like morphology in both subregions (Figure 6 G,H; GMko reduced by 32% in DG and 37% in CA1). Collectively, these results show overall reductions in dendritic complexity and suggest excitatory synaptic input to be reduced by approximately one third in the GM-CSF deficient hippocampus.

**GM-CSF deficiency does not decrease hippocampal long-term potentiation.** Long-term potentiation at Schaffer collaterals was not reduced in GMko mice (Figure 7A; wt,  $n = 21$  slices; GMko,  $n = 23$  slices;  $n = 8$  mice each), and I/O curves were identical in both groups (Figure 7B). Also, paired pulse analysis (20 ms delay) before and after induction of LTP revealed no differences, and showed the expected decrease in amplitude after LTP induction in both groups similar to measurements exemplified in previous work<sup>18</sup>. We conclude from these data that no major electrophysiological distortions are obvious in GM-CSF deficient animals.

**Cognitive effects of AAV-mediated manipulation of adult hippocampal GM-CSF signalling.** The constitutive knock-out of GM-CSF may alter neuronal development and, hence, cause secondary effects on behaviour and cognition. We therefore chose a second, independent approach of acute AAV-mediated somatic gene transfer in the adult hippocampus. Vectors were designed to overexpress (AAV-GMCSFR $\alpha$ ) or knock-down (AAV-sh427) hippocampal GM-CSFR $\alpha$  levels in adult mice, while a third group of animals received AAV vectors carrying a universal negative control construct (AAV-UNC) (Figure 8 A). Viral constructs led to robust hippocampal transduction based on reporter gene expression (Figure 8 B) and modulated hippocampal GM-CSFR $\alpha$  levels in the expected construct-dependent manner (Figure 8 C,D). While the knock-down construct led to a 42% decrease in GM-CSFR $\alpha$  levels, an approximate 10-fold overexpression was achieved by AAV-GMCSFR $\alpha$ .

No between-group differences of basal activity and anxiety levels were found in the open field (data not shown). When tested in the MWM, all groups showed similar performances during acquisition over 11 training days (Figure 9 A,B). However, recall in probe trial was dependent on viral constructs with the maximal time spent in the

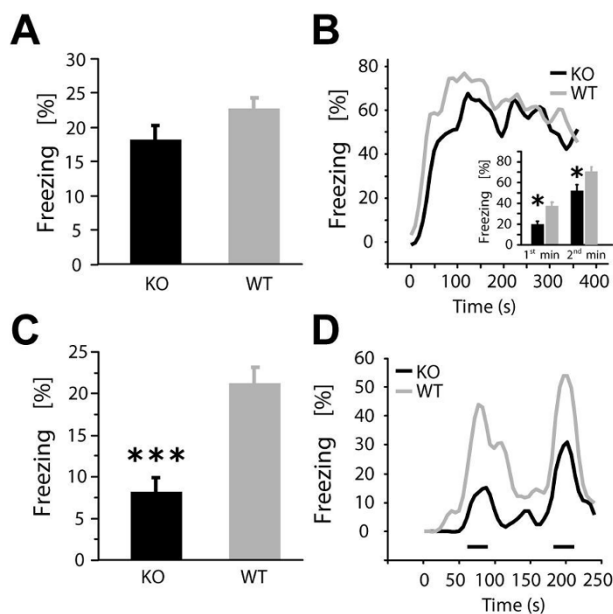


**Figure 4 | Effects of GM-CSF deficiency on fear memory formation.** (A) Freezing responses were identical during acquisition ( $p > 0.05$ ). (B) Context-challenge 24 hours after training elicited similarly substantial overall fear responses in both groups, however, with a significantly reduced amplitude in knock-outs during the first two minutes of exposure (inset,  $p < 0.001$  for both first and second minute). (C) Freezing responses to conditioned stimulus 48 hours after training were reduced in GMko mice indicating fear memory impairments in these animals ( $p < 0.001$ ). (D) Temporal analysis of cue-induced freezing 48 hours after training illustrates that differential fear responses are due to different response levels to cue presentations. Bars indicate duration of cue presentation. WT,  $n = 22$ ; KO,  $n = 21$  animals. Data is presented as mean  $\pm$  SEM.

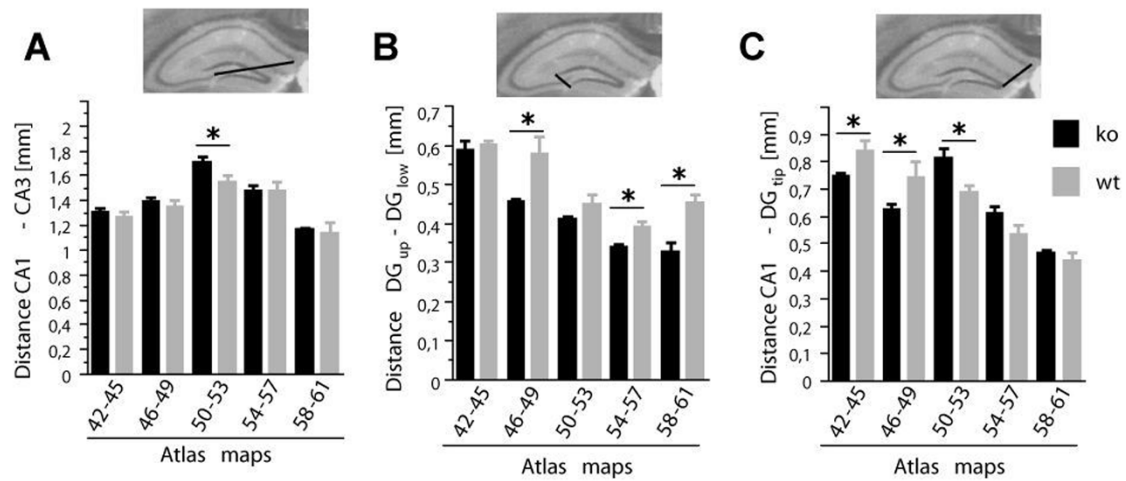


**Figure 5 | GM-CSF deficiency causes minor alterations in hippocampal anatomy.** (A) Distance between CA1 and CA4 ends of CA pyramidal cell layer was increased in the medial sections ( $p < 0.05$ ) but not in rostral, rostromedial, mediocaudal, and caudal sections of the hippocampal formation (all  $p > 0.05$ ). (B) Distance between open ends of upper and lower blade granule cell layers was decreased in the rostromedial, mediocaudal, and caudal sections (all  $p < 0.05$ ) but not in rostral and medial sections of the hippocampus (both  $p > 0.05$ ). (C) Distance between junction of upper and lower blade DG granule cell layers and the CA1 end of CA pyramidal cell layer was reduced in rostral and rostromedial sections (both  $p < 0.05$ ), increased in medial sections ( $p < 0.01$ ), and unaltered in mediocaudal and caudal sections of the hippocampus (both  $p > 0.05$ ). Labelling of x-axis in A–C denotes map numbers in<sup>48</sup>.  $n = 6$  animals per group. Data is presented as mean  $\pm$  SEM.

target area in AAV-GMCSFR $\alpha$  treated animals, and the minimal time spent in the AAV-sh427 treated animals (Figure 9 C, ANOVA,  $p = 0.05$ ; Tukey-Kramer HSD,  $p < 0.05$  for AAV-GMCSFR $\alpha$  vs. AAV-sh427;  $p > 0.05$  for UNC vs. AAV-GMCSFR $\alpha$  or AAV-sh427). Although there is a general correlation of spatial recall performance to the amount of receptor present, the absence of significant differences between control animals and the knock-down animals or overexpressors, respectively, does not give robust support for a role of GM-CSF in the adult animal at present.

## Discussion

The data reported here demonstrates that GM-CSF signalling plays an important role in processes underlying learning and memory formation. This conclusion is reached from assessing a broad array of cognitive functions in GM-CSF knock-out mice and partially supported from experiments in mice with targeted manipulation of hippocampal GM-CSF receptor  $\alpha$  levels.

GM-CSF deficient mice displayed broadly impaired learning and memory performances in an active avoidance paradigm, a water

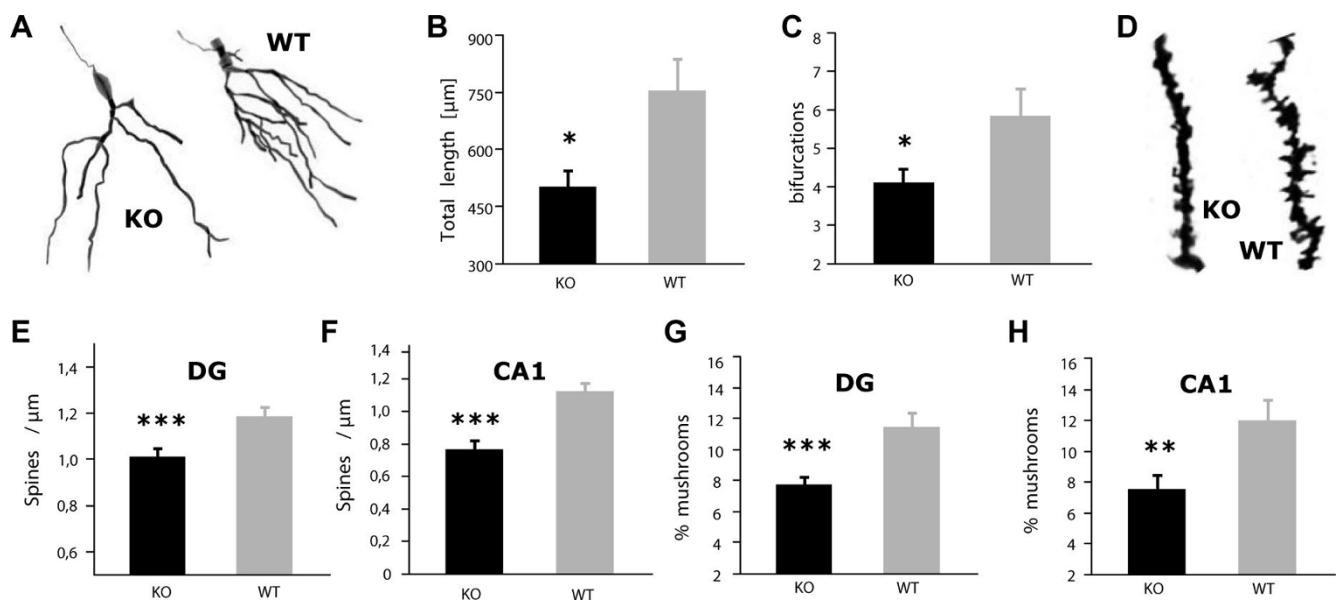


**Figure 6 | Effects of GM-CSF on neuronal complexity.** (A) Representative reconstructions of GMko and wildtype DG granule cells showing reduced complexity of GMko dendrites. (B,C) Quantification of total dendritic length and dendritic branch points of DG granule cells confirming rudimentary arborisation of GMko neurons. WT,  $n = 19$ ; KO,  $n = 17$  cells; 3 animals each. (D) Representative examples of dendrites from GMko and wildtype DG granule cells illustrating reduced spine density in knock-outs. (E,F) Spine density quantification of DG granule cells (str. moleculare) and CA1 pyramidal neurons (str. radiatum) showing reduced dendritic spine densities in both regions of the GMko brain. (G,H) Percentage of mushroom-shaped dendritic spines was reduced in both DG and CA1. (\*,  $p < 0.05$ ; \*\*,  $p < 0.01$ ; \*\*\*,  $p < 0.001$ ). E,G, WT,  $n = 25$ ; KO,  $n = 29$  cells; F,H, WT,  $n = 24$ ; KO,  $n = 25$  cells; 3 animals each. Data is presented as mean  $\pm$  SEM.

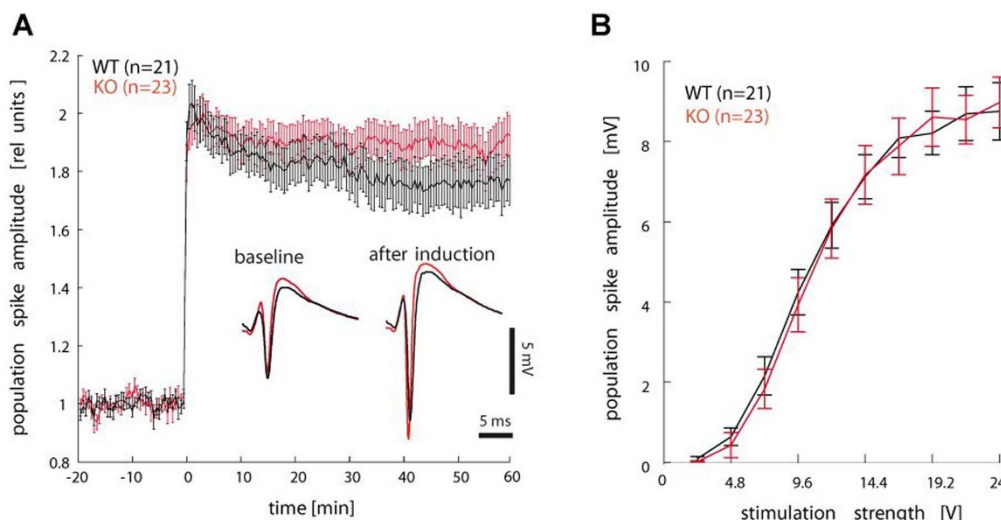


**Figure 7 | Long-term potentiation in the hippocampus of GM-CSF ko animals.** (A) LTP at CA3 Schaffer collaterals in the CA1 dendritic region was induced using a delta burst protocol at timepoint 0 min, and monitored for 60 min after induction. Shown are population spike amplitudes as means  $\pm$  SEM (wt, n = 21 slices; GMko, n = 23 slices; n = 8 mice each). GMko mice do not show impaired LTP induction when comparing the last 10 min of the protocol. Insets depict individual traces of wt and ko animals prior and after LTP induction. WT, n = 21; KO, n = 23 slices; 8 animals each. Data is presented as mean  $\pm$  SEM. (B) Input-output relation of electrical stimulation at the Schaffer collaterals. Shown are mean values of population spike amplitude and SEM of wild type (black) and knock out (red) at different stimulation strengths.

maze, and a fear conditioning experiment. These deficits were detected amongst a background of other behavioural alterations including reduced spontaneous locomotor activity which appeared to be caused by a diminished central drive for exploration in the absence of motor unit defects. While such activity reductions might perturb the interpretation of learning tasks, close behavioural analysis negates the existence of such conflict. For example, in the fear conditioning paradigm, low levels of activity could lead to overestimation of freezing behaviour and fear memory retention as the absence of motor activity during challenge with a previously shock-associated stimulus serves as the behavioural read-out of fear

memory formation. As we observed reduced rather than enhanced freezing responses in knock-outs, detection of locomotion-related false positive effects appears unlikely. Instead, diminished levels of activity might, if any, rather cause an underestimation of the fear memory deficit.

In the MWM, decreased activity could prolong escape latencies, and hence overshadow learning progress which might lead to false positive acquisition deficits. We circumvented this problem by using escape path length as a swim speed-independent parameter that is gradually reduced during acquisition through increasingly direct trajectories. Moreover, absence of both visual and motivational

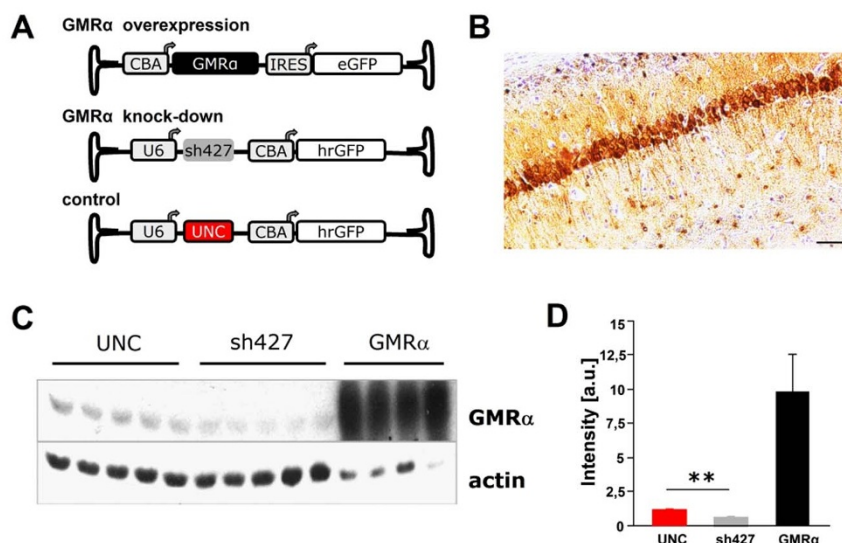


**Figure 8 | AAV-mediated transgene delivery to the adult murine hippocampus for bidirectional manipulation of GM-CSFR $\alpha$  levels in wildtypes.** (A) Vectors employed in this study. (B) Representative example of robust hippocampal reporter gene expression (AAV-UNC; CA1 region). Reference bar, 50  $\mu$ m. (C) GM-CSFR $\alpha$  levels in western blots of AAV-treated hippocampal samples differ in the expected construct-dependent manner. (D) Quantification of blot in (B). (\*\*,  $p < 0.01$ ) CBA, chicken beta actin promoter; GMR $\alpha$ , GM-CSF receptor alpha subunit; IRES, internal ribosome entry site; eGFP, enhanced green fluorescent protein; U6, human U6 promoter; shRNA, small hairpin RNA; hrGFP, humanized renilla green fluorescent protein; UNC, universal negative control. Data is presented as mean  $\pm$  SEM.

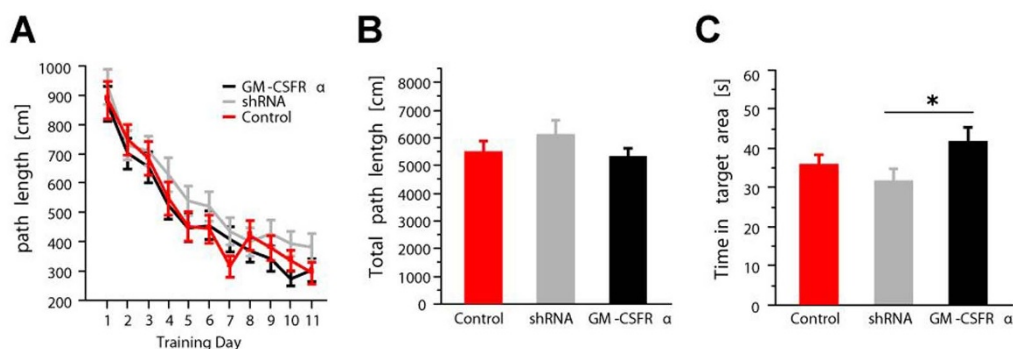


**Figure 9** | Impact of AAV-mediated manipulation of hippocampal GM-CSFR $\alpha$  levels on spatial learning and memory. (A) Learning curves during training were indistinguishable between groups (genotype\*day  $p > 0.05$ ). (B) Area under the curve plot of spatial learning in the MWM (genotype  $p > 0.05$ ). (C) Accuracy of memory for the former platform location during the probe trial was dependent on hippocampal GM-CSFR $\alpha$  levels with an impairment and improvement caused by treatment with AAV-sh427 and AAV-GMCSFR $\alpha$ , respectively, as judged by the time spent in the target area. (\*,  $p < 0.05$ ).  $n = 18$  animals per group. Data is presented as mean  $\pm$  SEM.

deficits to mount the platform during visually cued trials further indicates that deficits of GMko mice were correctly ascribed to spatial memory impairments. While we observed exploratory deficits in three independent mildly or non-aversive tests (open field, LABORAS, dark-light box), we found that this did not translate into reduced readiness to evade the highly aversive environment of the MWM. We also did not encounter any behavioural features in the other aversion-driven learning and memory paradigms that would have indicated motivational deficits, despair, or anhedonia. The motivational deficits observed in low or non-aversive settings, therefore, did not interfere with performance in aversive settings which apparently led to disinhibition of voluntary activity in knock-out animals.

Rotarod testing further confirmed the physical capability of knock-outs to master the cognition tasks while also revealing potential effects of GM-CSF on motor function. The data suggest a better baseline performance in the absence of GM-CSF, although the learning curve may be better in controls. The reason for this is unclear at present. A number of components contribute to performance in this type of repeated rotarod assay (motor strength, coordination, endurance, and motor learning) and could be potentially involved in the effects seen. GM-CSF  $\alpha$  receptors are expressed in both cerebellar Purkinje cells and neurons of the motor cortex<sup>7</sup>, but little is known on muscle expression of the GM-CSF system. This interesting observation warrants further studies on the role of GM-CSF in the motor system.

In summary, inferior performance of GMko mice in our cognitive behavioural test battery therefore appears due to genuine learning and memory deficits. Strikingly, such deficits were observed in both hippocampus and amygdala-dependent tasks, indicating important functions for the GM-CSF system in both brain regions.

The cognitive deficit of GMko mice was paralleled by hippocampal reductions of dendritic complexity. We observed decreased dendritic spine densities and a relative loss of the likely more mature mushroom-shaped spines<sup>19</sup> in the CA1 and DG subfields. These alterations provide a convincing morphological explanation for the impairments in learning and memory performance observed in these animals as they greatly limit the capacity of principal neurons to partake in neuronal networks involved in encoding task-specific memory traces. We have shown previously that Akt, stat3 and Erk pathways are activated by GM-CSF in neurons<sup>7</sup>. Both PI3K/Akt and MAPK/Erk pathways have been implicated in dendritic size and complexity regulation<sup>20–22</sup>, and therefore present likely candidates to mediate the observed effects of GM-CSF in dendritic morphology.

Despite these morphological limitations we did not observe a reduction in long-term potentiation (LTP). Obviously, the EPSP generated by fewer synaptic inputs in the markedly pruned dendritic

tree of CA1 pyramidal neurons is relatively larger than the one elicited in wildtype neurons, possibly because of the smaller surface area and volume of the dendrites. The GMko animals are therefore an interesting counterexample for the often assumed straight correlation of LTP and learning and memory performance, and underline that the relationship between the two phenomena is much more complicated<sup>23</sup>. There are a number of examples in the literature for discordant data in LTP and learning tasks e.g.<sup>24–26</sup> that support the notion that LTP does not equal memory performance.

The relevance of neuronal GM-CSF signalling for cognitive functions was further investigated by an independent and complementary *in vivo* approach using AAV vectors. Here, in contrast to the knock-out mice, the receptor was targeted, the manipulation was confined to the hippocampus, and the alterations occurred only after animals had reached adulthood. Although spatial memory of GM CSFR $\alpha$  overexpressing mice was significantly enhanced compared to GM CSFR $\alpha$  knock down animals, we could not demonstrate a significant difference when contrasting controls to the overexpressors or knock-down animals.

We therefore conclude that chronic absence of GM-CSF has a strong effect on learning and memory, but that relatively acute manipulation of the GM-CSF system in the adult fail to generate similar effect sizes.

Future studies are needed to dissect how strong the developmental component of the effect is, and whether longerlasting changes of the GM-CSF system in the adult will show clear effects on spatial learning. While the strong morphological alterations in the dendritic structure of knock out mice are likely one component of the long term alteration of the GM-CSF system, it remains to be defined what physiological and ultrastructural changes occur in the more acute manipulations of this system in adults, if any.

GM-CSF belongs to the group of hematopoietic growth factors as do granulocyte-colony stimulating factor (G-CSF) and erythropoietin (EPO). Recently, neuronal receptor expression for all of these growth factors has been demonstrated with particularly high expression levels in cortical and hippocampal neurons<sup>7,27,28</sup>. Subcutaneous injections of G-CSF improved spatial learning in wildtype rats<sup>29</sup> while, conversely, a phenotypic analysis of G-CSF knock-out mice revealed disruptions of memory formation along with decreased neuronal complexity in the hippocampus<sup>30</sup>. Intraperitoneal EPO injections enhanced hippocampus-dependent memory in wildtype mice<sup>31,32</sup>. This was also observed in transgenic mice expressing constitutively active EPO receptors in cortical and hippocampal pyramidal neurons<sup>33</sup>. Clinical studies with EPO suggest that these findings may be translatable to patients with cognitive problems<sup>34–36</sup>. Our data establish that the group of these hematopoietic factors as a whole shares highly analogous functions in the CNS, extending from basic



anti-apoptotic to high level neuronal network functions. These properties are shared with other neurotrophic factors such as BDNF which is known as a key determinant for memory formation and synaptic strength in the hippocampus<sup>37,38</sup>.

Collectively, our results suggest that GM-CSF signalling plays a hitherto unrecognized role in learning and memory. Unlike most other neurotrophic proteins, GM-CSF is able to pass the intact blood-brain barrier, and is well-tolerated in humans. Both deficit of ligand and receptor leads to reduced memory performance, and the AAV experiment suggests that memory recall improves with the level of GM-CSF receptor expression. GM-CSF therefore appears as a bona fide candidate for improvement of cognitive deficits, although we have not tested peripherally applied GM-CSF here. It is interesting in this regard that peripheral application of GM-CSF counteracted scopolamine-induced acute cognitive deficits<sup>39</sup>, and that a recent report by Boyd and co-workers indicated that GM-CSF treatment was able to reverse cognitive deficits in a mouse model of Alzheimer's disease<sup>40</sup>. Although these authors ascribed the beneficial effect of GM-CSF treatment to the reduction of amyloidosis, it is tempting to assume in the light of our findings that direct effects on cognitive processing were involved.

## Methods

**Animals.** Experiments were conducted on adult male mice housed in groups of 3–5 under standard conditions on a 12-h light/dark cycle with lights on at 7:00 AM and water and food available *ad libitum*. The GM-CSF-deficient mouse line was a gift from Jeffrey A. Whitsett of the Cincinnati Children's Hospital Medical Center and has previously been described in many studies<sup>41–43</sup>. Wildtype C57Bl/6 mice were obtained from Charles River (CRL, Sulzfeld, Germany). All animal experimentation was approved by Regierungspräsidium Karlsruhe as the responsible local authority.

**Design of AAV expression constructs.** The vector for GM-CSFR $\alpha$  overexpression was based on expression cassette pAAV-CBA-pl-IRES-EGFP-WPRE-bGHpA containing a CMV immediate early enhancer / chicken  $\beta$ -actin hybrid promoter (CBA), a polylinker (pl), an IRES element, the EGFP cDNA, the woodchuck hepatitis virus post-transcriptional regulatory element (WPRE), and the bovine growth hormone polyadenylation sequence (bGHpA). This cassette was flanked by AAV2 inverted terminal repeats (ITRs). Vector AAV-GMCSFR $\alpha$  was constructed by amplification of the murine GM-CSFR $\alpha$  ORF using primers GMCSFR $\alpha$ \_s (GGGGACAAGTTTGTACAAAAAAGCAGGCTACCATGGCAGGAAGCC-CCCTGTCTC) and GMCSFR $\alpha$ \_as (GGGGACCACTTTGTACAAGAAA-GCTGGGTCCTAGGGCTGCAGGAGGTCCTTC), followed by subcloning into the pl site. Vectors for small hairpin RNA (shRNA) expression were based on AAV2 ITR-flanked shRNA expression cassette pAM/U6-pl-CBA-hrGFP-WPRE-BGHpA described earlier<sup>44</sup>. This vector harbours a CBA-controlled humanized renilla GFP (hrGFP) reporter gene along with a shRNA expression cassette containing the human U6 promoter. For knock-down of GM-CSFR $\alpha$  transcript levels, target sequence GGAGGCTGAGCTTCGTCACAG was identified with Invitrogen's BLOCK-iT™ RNAi Designer web tool, and complementary DNA oligonucleotides encoding shRNAs directed against this target sequence were generated using Ambion's pSilencer™ Expression Vectors Insert Design Tool. For the loop structure, sequence GTGAAGCCACAGATG was used as described previously<sup>45</sup>. Based on the location of the target sequence in the GM-CSFR $\alpha$  ORF, the resulting vector was termed AAV-sh427. The same expression cassette was used to generate a control vector driving expression of the universal negative control shRNA "UNC" with the validated non-targeting sequence ACTACCGTTGTTATAGGTG<sup>46</sup>.

**Production of AAV.** Chimeric AAV vectors containing AAV serotype 1 and 2 capsid proteins in a 1:1 ratio were generated as described earlier<sup>47</sup>. Briefly, HEK293 cells were CaPO<sub>4</sub>-transfected with the respective AAV expression plasmid, adenoviral helper plasmid (pFA6) and equal amounts of both AAV1 (pH21) and AAV2 (pRV1) helper plasmids. Cells were harvested sixty hours following transfection and vectors were purified using heparin affinity columns (HiTrap Heparin HP; Amersham Pharmacia Biotech, Uppsala, Sweden). Quantitative PCR (SYBR-Green; Lightcycler™, Roche Diagnostics) using primers derived from WPRE sequence were used for genomic titration of vector preparations.

**Stereotaxic surgery.** For AAV-treatment, 54 adult male C57Bl/6 mice (25–30 g) were randomly assigned to three groups of 18 animals. Mice were anesthetized by i.p. injection of a mixture of ketamine (120 mg/kg body weight; Pharmanovo, Hannover, Germany) and xylazine (Rompun, 16 mg/kg body weight; Bayer, Leverkusen, Germany), and placed in a stereotaxic frame (David Kopf Instruments, Tujunga, CA) before receiving bilateral infusions of 1.5  $\mu$ l vector solution at a flow rate of 150 nl/min through a 35 G stainless steel beveled NanoFil needle (WPI, Berlin, Germany) to the dorsal hippocampus. Coordinates relative to bregma at skull level were RC -2.0 mm, ML  $\pm$ 2.0 mm, DV -2.0 mm<sup>48</sup>. Following infusion, needles were left in place

for 2 min to allow fluid distribution away from the injection site depot. After surgery, mice were left in their home cages for 3 weeks to allow AAV-mediated transgene expression to reach stable peak levels.

**Behavioural testing.** Animals for the knock-out study were subdivided into two cohorts to be analyzed in individual test batteries, respectively. Cohort #1 (wt and ko n = 22 and 21 animals, respectively, 8 weeks old at beginning of testing) was used for open field, rotarod, dark-light box, plantar pain threshold, and LABORAS testing, while cohort #2 (wt and ko n = 18 and 16 animals, 10 weeks old at beginning of testing) was used for learning and memory paradigms consisting of active place avoidance, fear conditioning, and Morris water maze. This design helped avoid excessive use of subjects as well as carry-over effects from aversion-driven cognitive tests to paradigms assessing spontaneous behaviours. All tests were separated by >1 week while >4 weeks were allowed between fear conditioning and water maze. AAV-treated animals were first tested in the open field and then in the MWM. All animals were handled for >2 weeks prior to testing. Additionally, mice awaiting testing were physically separated from the testing environment to prevent them from perceiving (ultrasonic) distress calls or stress-induced pheromone secretion from subjects undergoing testing. After testing, animals were placed in holding cages before returning to their home cages to limit their influence on yet untested animals which might become alert by odor, vocalization, or behavioural alterations of tested animal.

**Open field.** Locomotor activity was measured in an open field (40 $\times$ 40 $\times$ 40 cm) located in a dedicated testing cubicle and homogeneously illuminated at light intensities well below aversive levels (40–50 lx). Animals were introduced to the center of the arena and allowed to freely explore for 30 min. Movement was tracked via a top-mounted video camera connected to proprietary high-resolution tracking software (SYGNIS tracker v4.1.4). Analysis was based on both a virtual grid subdividing the arena into 25 squares of 64 cm<sup>2</sup> each and a circle with radius r = 12 cm around the center of the arena. Total distance and time spent in the circular center and the four corner squares of the open field were recorded.

**Active place avoidance.** The active place avoidance apparatus<sup>49</sup> was located in a testing cubicle providing visual cues. It consisted of a rotating (1 rpm) circular platform (r = 40 cm) surrounded by a transparent wall. One randomly chosen 60° sector was designated as the non-rotating shock zone where animals received a 0.4 mA electric shock upon entry, and further identical shocks every 1.5 s after failure to leave the sector. For mice, this sector was only identifiable relative to the extra-maze visual cues. Due to platform rotation, passive strategies were inevitably associated with foot-shocks, and animals quickly learned to actively avoid the sector. After a 10 min pre-training session without shocks, eight 10 min training trials were conducted at intervals of 12 min which animals spent in their home cages. After 24 hours, one retention trial was run (shocker off). Latency to shock zone entry was recorded during all trials.

**Fear conditioning.** For acquisition, mice spent 6 min inside a conditioning chamber (Med Associates Inc., St. Albans, Vermont) and were exposed to an acoustic signal (5 kHz, 85 dB, 30 s) at 90–120 s, 150–180 s, 210–240 s, and 270–300 s (conditioned stimulus, CS). At the last second of each tone segment, one foot shock (0.6 mA, 1 s) was applied via the floor grid (unconditioned stimulus, US). Freezing behaviour was analyzed via a video camera connected to video tracking software (Med Associates Inc, St. Albans, Vermont), and was defined as a change in <11 of 76800 pixels between adjacent frames (33 ms apart) over a time period of >1 s. After 24 hours, animals were re-introduced to the chamber for 6 min in the absence of CS or US to evaluate contextual fear memory. 48 hours after training, cue-related fear memory was assessed. To hinder recognition of the chamber from haptic, olfactory, or visual cues the chamber was remodelled with a flat plastic floor panel covering the steel grid and a black roof-shaped insert, by replacement of visible light with near infrared illumination, and by use of a different disinfectant for cleaning. Mice were exposed to this altered context for 4 min during which the 30 s CS was presented twice, terminating at 60 and 180 s, respectively. Locomotor behaviour was analyzed as before.

**Morris water maze (MWM).** A standard hidden platform protocol was employed. The circular pool (r = 85 cm) was filled with opaque water (24  $\pm$  1°C) to a height of 35 cm and a circular escape platform (r = 5 cm) was submerged 1 cm below the water surface at a constant position in the center of the North-West (NW) quadrant during training. The pool openly faced the testing room which provided ample distal cues for visual spatial navigation. To reduce stress effects<sup>50</sup>, mice were habituated to the maze 24 hours prior to training (4 trials, visible platform located once in every quadrant). Training consisted of 4 daily trials on 11 (AAV cohort) or 12 (GMko cohort) consecutive days at inter-trial intervals (ITI) of 90 min. Cages were placed under infra-red lamps during the first 45 min of the ITI to prevent hypothermia. Animals were introduced to the pool from start positions East (E), South-East (SE), South (S), and South-West (SW) to avoid close initial proximity to platform. Starting positions were block-randomized with all possible starting positions in random order on every day. After mounting the platform, animals were left there for 15 s. Cut-off time for trials was set to 60 s after which animals failing to locate the platform were guided with a wooden rod and also left there for 15 s. Abandoning the platform was considered a platform jump-off. One probe trial of 120 s with the platform removed from the pool was conducted 24 hours after the last training day. Here, animals entered the pool from position S. On the following day, a cued platform test was





conducted to rule out gross visual deficits. This test was similar to the pre-training session except that black curtains shielded the pool from extra-maze cues to prevent animals from adopting previously learned search strategies. GMko analysis additionally comprised an additional 5-day reversal learning protocol starting 48 hours later. Here, all positions were inverted compared to the former setup, i.e. platform now at SE and starting points at W, NW, N, and NE. Frequency density maps were generated using a module of SYGNIS tracker v4.1.4 by accumulative addition of tracked trajectories (1 pixel wide) such that pixel density was analyzed in blocks of 5×5 pixels and normalized to performance of wildtypes at the last training day.

**Rotarod.** Animals were tested for motor function on a rotarod (Ugo Basile, Comerio, Italy) on 6 consecutive days with 5 daily trials at ITIs of 8 min using a challenging constant acceleration protocol (4–80 rpm over 300 s). Fall-off latencies were recorded. Co-variate analysis of body weight effects was conducted using mean of weights obtained before and after testing.

**Dark-light emergence test.** The apparatus consisted of a white 42×42×33 cm open field connected via a 8.5×10 cm door at floor level at the center of one side to a black 21×42×33 cm compartment which was lid-covered to keep it dark whereas the open field was brightly illuminated (center: 120 lx, junction door: 95 lx). Mice were placed into the dark compartment for a 60 s habituation period with the exit closed. Thereafter, the door was opened and animals were left to freely explore for 330 s. Time spent in the lit compartment with all paws and number of rearings were recorded.

**Plantar pain threshold.** Plantar pain threshold of rear paws was assessed using a Hargreaves apparatus (Ugo Basile, Comerio, Italy) to measure responses to infrared (IR) stimulation (220 mW/cm<sup>2</sup>) over 5 trials with ITIs of 10 min. As this test required animal's hind paws to rest motionless, test chamber habituation was allowed for >15 min. Care was taken to only test animals in alert, yet immobile states with dry paws. If initiated trials were interrupted by paw movement related to grooming or locomotion, trials were re-started no earlier than 10 min later to allow for reversal of any pain sensitization triggered during the failed attempt.

**Spontaneous behaviour assessment using LABORAS.** The Laboratory Animal Behaviour Observation, Registration and Analysis System (LABORAS, Metris, Hoofddorp, Netherlands) is a fully automated system for the vibration and force pattern-based detection and discrimination of a variety of rodent behaviours including locomotion, immobility, and cage climbing. Mice were individually placed in LABORAS cages at 6:00 h PM and spontaneous behaviour was monitored for 12 hours starting at 7:00 h PM.

**Hippocampal anatomy.** After deep anaesthesia, GMko and wildtype mice (n = 6 per group) were transcardially perfused with 4% paraformaldehyde. Brains were removed, embedded in paraffin and cut on a microtome to 10 µm coronal sections of which always three consecutive slices were mounted to one microscope slide. Starting with the rostralmost hippocampal section, every 10<sup>th</sup> slide was subjected to Trichrom staining (Sigma Aldrich, Steinheim, Germany) such that 9 slides (27 sections) were skipped. Using a mouse brain atlas<sup>48</sup>, slides not corresponding to region −1.34 mm to −3.64 mm relative to bregma were excluded from further analysis. After tissue digitization, hippocampal areas were determined using ImageJ software and hippocampal volumes were calculated from these values by the Cavalieri method using equation  $V = \sum(A_1, A_2, \dots, A_n) * d$ , where V = hippocampal volume, A<sub>x</sub> = mean hippocampal area of three sections on slide x, and d = distance between sections on consecutive slides (270 µm). Next, sections were subdivided into five groups (G1–G5) of rostral (G1), rostro-medial (G2), medial (G3), medio-caudal (G4), and caudal (G5) location with a rostro-caudal extent of 0.36 to 0.4 mm each. Within groups, lengths of distances D1–D5 between characteristic hippocampal structures were determined. These were defined as follows: D1 = maximal interhemispheric distance between CA3 pyramidal cell nuclei; D2 = distance between dorsal tips of DG granule cell and CA1 pyramidal cell layers; D3 = distance between ends of CA cell layer (CA1–CA4); D4 = distance between open ends of DG upper and lower blades; D5 = distance between CA1 end of CA cell layer and junction of DG upper and lower blades. However, D1 and D2 were only determined on the one section per animal in which hippocampal width was maximal and no CA3 pyramidal cell nuclei lay ventral relative to DG granule cell nuclei.

**Neuronal morphology and spine analysis.** Brains removed from deeply anesthetized animals were subjected to Golgi-Cox staining with FD Rapid GolgiStain kit (FD NeuroTechnologies, Ellicott City, USA) according to manufacturer's instructions. Confocal microscopic image acquisition was performed with a Leica TCS-SP5 laser scanning microscope (Leica Microsystems, Wetzlar, Germany) on 100 µm cryosections. Whole neuron reconstruction was performed on image stacks (step size 0.5 µm) of individual DG granule cells using Neuromatic software v1.6.3. Likewise, spines of both CA1 pyramidal and DG granule cells were analyzed on image stacks (step size 0.2 µm) of first order dendritic bifurcations in stratum radiatum (CA1) or stratum moleculare (DG). Spine analysis was performed towards the distal tip of the neurite, either until the neurite ended, disappeared from the display window, or branched again.

**Electrophysiology.** Experiments were performed on 24 mice (8.2 ± 1.4 wks). Brains were removed from CO<sub>2</sub>-anesthetized animals and were kept in 1–4°C artificial cerebrospinal fluid (ACSF), containing (mM): NaCl 124, KCl 3, MgSO<sub>4</sub> 1.8, CaCl<sub>2</sub> 1.6, glucose 10, NaH<sub>2</sub>PO<sub>4</sub> 1.25, NaHCO<sub>3</sub> 26, saturated with 95% O<sub>2</sub>/5% CO<sub>2</sub> at pH 7.4 at 35°C. Horizontal hippocampal slices (450 µm) were cut on a vibratome (Leica, VT 1000S, Germany), maintained at 35 ± 0.5°C in a Haas-type interface chamber, and rested for ≥2.5 hours prior to experiments. Extracellular glass microelectrodes (tip diameter ~5 µm) filled with ACSF were placed in CA1 str. pyramidale and str. radiatum. Electrical stimulation to Schaffer collaterals was achieved by a bipolar platinum/iridium electrode (Science Products, 100 kΩ at 1 kHz, 75 µm tip distance). Stimulation strength was adjusted to evoke population spikes with half-maximal amplitudes. Test pulses were applied every 30 s. LTP was induced by a delta burst protocol (Ten bursts over 8 s, each 100 Hz and 40 ms). If baseline recording was for ≥20 min, potentials were amplified 100-fold, low and high pass-filtered at 10 kHz and 0.3 Hz (EXT10-2FX amplifiers, npi electronics, Tamm, Germany), respectively, digitized at 20 kHz (1401 interface and Spike-2 software, CED, Cambridge, UK), and analyzed offline using custom routines written in Matlab (The MathWorks, Natick, MA). For I/O curves, maximal population spike responses of individual slices were determined by increasing stimulation strength in 2.4 V steps until field potential amplitudes were maximal. Population spike amplitudes for different stimulation strengths were averaged across slices. As only a minority of slices reached higher stimulation strengths, averaging was terminated if less than 1/3 of slices were stimulated with that specific stimulation strength. This resulted in maximal stimulation strength of 24 V for mean I/O curves. Then, stimulation strength was adjusted to evoke population spikes with 50% of the maximal amplitude.

**Neurite outgrowth analysis.** Primary hippocampal neurons were prepared from E18.5 rat embryos and seeded on coverslips in 24-well plates (10,000 cells / well). Six hours later, GM-CSF or vehicle was added. Neurons were fixed with 4% paraformaldehyde 48 hours after stimulation. Cells were stained for neurofilament-L (AB9568, 1 : 200, Millipore, Schwalbach, Germany) in 1% BSA/TBS o/n at 4°C. FITC-labelled secondary antibody was applied for 1 h at room temperature in 0.1% BSA/TBS (1 : 200, Dianova, Hamburg, Germany). Image acquisition at 40x magnification was done in grids of 7×7 pictures to yield composites of 49 images covering a total of 1.8 mm<sup>2</sup>. Each composite was screened in a predefined pattern by a blinded observer for fully traceable neurons and total neurite lengths were determined using ImageJ plug-in NeuronJ. A maximum of 15 neurons were traced per coverslip to ultimately yield 100 neurons per group.

**Statistics.** All data are presented as mean ± SEM. Comparisons between two conditions were made using two-sided t-test. More conditions were analyzed using ANOVA with a post-hoc Tukey-Kramer test. Serial tests were analyzed using regression analysis. In addition, AUC analyses were performed. P-values ≤ 0.05 were considered significant for all tests. All analyses were performed using JMP v8.02 (SAS Institute).

1. Armitage, J. O. Emerging applications of recombinant human granulocyte-macrophage colony-stimulating factor. *Blood* **92**, 4491–508 (1998).
2. Metcalf, D. The molecular control of cell division, differentiation commitment and maturation in haemopoietic cells. *Nature* **339**, 27–30 (1989).
3. Hansen, G. *et al.* The structure of the GM-CSF receptor complex reveals a distinct mode of cytokine receptor activation. *Cell* **134**, 496–507 (2008).
4. Baker, J., McCune, J. S., Harvey, R. D. 3rd, Bonsignore, C. & Lindley, C. M. Granulocyte colony-stimulating factor use in cancer patients. *Ann Pharmacother* **34**, 851–7 (2000).
5. Disis, M. L. Clinical use of subcutaneous G-CSF or GM-CSF in malignancy. *Oncology (Williston Park)* **19**, 5–9 (2005).
6. Korzenik, J. R., Dieckgraefe, B. K., Valentine, J. F., Hausman, D. F. & Gilbert, M. J. Sargramostim for active Crohn's disease. *N Engl J Med* **352**, 2193–201 (2005).
7. Schabitz, W. R. *et al.* A neuroprotective function for the hematopoietic protein granulocyte-macrophage colony stimulating factor (GM-CSF). *J Cereb Blood Flow Metab* **28**, 29–43 (2008).
8. Kong, T. *et al.* Reduction in programmed cell death and improvement in functional outcome of transient focal cerebral ischemia after administration of granulocyte-macrophage colony-stimulating factor in rats. Laboratory investigation. *J Neurosurg* **111**, 155–63 (2009).
9. Nakagawa, T., Suga, S., Kawase, T. & Toda, M. Intracarotid injection of granulocyte-macrophage colony-stimulating factor induces neuroprotection in a rat transient middle cerebral artery occlusion model. *Brain Res* **1089**, 179–85 (2006).
10. Kim, N. K. *et al.* Granulocyte-macrophage colony-stimulating factor promotes survival of dopaminergic neurons in the 1-methyl-4-phenyl-1,2,3,6-tetrahydropyridine-induced murine Parkinson's disease model. *Eur J Neurosci* **29**, 891–900 (2009).
11. Kruger, C., Laage, R., Pitzer, C., Schabitz, W. R. & Schneider, A. The hematopoietic factor GM-CSF (granulocyte-macrophage colony-stimulating factor) promotes neuronal differentiation of adult neural stem cells in vitro. *BMC Neurosci* **8**, 88 (2007).
12. Reed, J. A. *et al.* GM-CSF action in the CNS decreases food intake and body weight. *J Clin Invest* **115**, 3035–44 (2005).



13. Maurer, M. H., Schabitz, W. R. & Schneider, A. Old friends in new constellations-- the hematopoietic growth factors G-CSF, GM-CSF, and EPO for the treatment of neurological diseases. *Curr Med Chem* **15**, 1407–11 (2008).
14. McLay, R. N., Banks, W. A. & Kastin, A. J. Granulocyte macrophage-colony stimulating factor crosses the blood-testis barrier in mice. *Biol Reprod* **57**, 822–6 (1997).
15. Aboulkassim, T. *et al.* Ligand-dependent TrkA activity in brain differentially affects spatial learning and long-term memory. *Mol Pharmacol* **80**, 498–508 (2011).
16. Bekinschtein, P. *et al.* BDNF is essential to promote persistence of long-term memory storage. *Proc Natl Acad Sci U S A* **105**, 2711–6 (2008).
17. Dranoff, G. *et al.* Involvement of granulocyte-macrophage colony-stimulating factor in pulmonary homeostasis. *Science* **264**, 713–6 (1994).
18. Weiss, E. K., Krupka, N., Bahner, F., Both, M. & Draguhn, A. Fast effects of glucocorticoids on memory-related network oscillations in the mouse hippocampus. *J Neuroendocrinol* **20**, 549–57 (2008).
19. Matsuzaki, M. *et al.* Dendritic spine geometry is critical for AMPA receptor expression in hippocampal CA1 pyramidal neurons. *Nat Neurosci* **4**, 1086–92 (2001).
20. Kumar, V., Zhang, M. X., Swank, M. W., Kunz, J. & Wu, G. Y. Regulation of dendritic morphogenesis by Ras-PI3K-Akt-mTOR and Ras-MAPK signaling pathways. *J Neurosci* **25**, 11288–99 (2005).
21. Jan, Y. N. & Jan, L. Y. Branching out: mechanisms of dendritic arborization. *Nat Rev Neurosci* **11**, 316–28 (2010).
22. Jaworski, J., Spangler, S., Seeburg, D. P., Hoogenraad, C. C. & Sheng, M. Control of dendritic arborization by the phosphoinositide-3'-kinase-Akt-mammalian target of rapamycin pathway. *J Neurosci* **25**, 11300–12 (2005).
23. Neves, G., Cooke, S. F. & Bliss, T. V. Synaptic plasticity, memory and the hippocampus: a neural network approach to causality. *Nat Rev Neurosci* **9**, 65–75 (2008).
24. Kim, M. H. *et al.* Enhanced NMDA receptor-mediated synaptic transmission, enhanced long-term potentiation, and impaired learning and memory in mice lacking IRSp53. *J Neurosci* **29**, 1586–95 (2009).
25. Migaud, M. *et al.* Enhanced long-term potentiation and impaired learning in mice with mutant postsynaptic density-95 protein. *Nature* **396**, 433–9 (1998).
26. Rutten, K. *et al.* Enhanced long-term potentiation and impaired learning in phosphodiesterase 4D-knockout (PDE4D) mice. *Eur J Neurosci* **28**, 625–32 (2008).
27. Digicaylioglu, M. *et al.* Localization of specific erythropoietin binding sites in defined areas of the mouse brain. *Proc Natl Acad Sci U S A* **92**, 3717–20 (1995).
28. Schneider, A. *et al.* The hematopoietic factor G-CSF is a neuronal ligand that counteracts programmed cell death and drives neurogenesis. *J Clin Invest* **115**, 2083–98 (2005).
29. Diederich, K. *et al.* Synergetic effects of granulocyte-colony stimulating factor and cognitive training on spatial learning and survival of newborn hippocampal neurons. *PLoS One* **4**, e5303 (2009).
30. Diederich, K. *et al.* The role of granulocyte-colony stimulating factor (G-CSF) in the healthy brain: a characterization of G-CSF-deficient mice. *J Neurosci* **29**, 11572–81 (2009).
31. Adamcio, B. *et al.* Erythropoietin enhances hippocampal long-term potentiation and memory. *BMC Biol* **6**, 37 (2008).
32. El-Kordi, A., Radyushkin, K. & Ehrenreich, H. Erythropoietin improves operant conditioning and stability of cognitive performance in mice. *BMC Biol* **7**, 37 (2009).
33. Sargin, D. *et al.* Expression of constitutively active erythropoietin receptor in pyramidal neurons of cortex and hippocampus boosts higher cognitive functions in mice. *BMC Biol* **9**, 27 (2011).
34. Ehrenreich, H. *et al.* Exploring recombinant human erythropoietin in chronic progressive multiple sclerosis. *Brain* **130**, 2577–88 (2007).
35. Ehrenreich, H. *et al.* Improvement of cognitive functions in chronic schizophrenic patients by recombinant human erythropoietin. *Mol Psychiatry* **12**, 206–20 (2007).
36. Marsh, J. T. *et al.* rHuEPO treatment improves brain and cognitive function of anemic dialysis patients. *Kidney Int* **39**, 155–63 (1991).
37. Korte, M. *et al.* Virus-mediated gene transfer into hippocampal CA1 region restores long-term potentiation in brain-derived neurotrophic factor mutant mice. *Proc Natl Acad Sci U S A* **93**, 12547–52 (1996).
38. Korte, M., Kang, H., Bonhoeffer, T. & Schuman, E. A role for BDNF in the late-phase of hippocampal long-term potentiation. *Neuropharmacology* **37**, 553–9 (1998).
39. Bianchi, M., Sacerdote, P. & Panerai, A. E. Peripherally administered GM-CSF interferes with scopolamine-induced amnesia in mice: involvement of interleukin-1. *Brain Res* **729**, 285–8 (1996).
40. Boyd, T. D. *et al.* GM-CSF upregulated in rheumatoid arthritis reverses cognitive impairment and amyloidosis in Alzheimer mice. *J Alzheimers Dis* **21**, 507–18 (2010).
41. Berclaz, P. Y. *et al.* GM-CSF regulates a PU.1-dependent transcriptional program determining the pulmonary response to LPS. *Am J Respir Cell Mol Biol* **36**, 114–21 (2007).
42. LeVine, A. M., Reed, J. A., Kurak, K. E., Cianciolo, E. & Whitsett, J. A. GM-CSF-deficient mice are susceptible to pulmonary group B streptococcal infection. *J Clin Invest* **103**, 563–9 (1999).
43. Yoshida, M., Ikegami, M., Reed, J. A., Chronoes, Z. C. & Whitsett, J. A. GM-CSF regulates protein and lipid catabolism by alveolar macrophages. *Am J Physiol Lung Cell Mol Physiol* **280**, L379–86 (2001).
44. Franich, N. R. *et al.* AAV vector-mediated RNAi of mutant huntingtin expression is neuroprotective in a novel genetic rat model of Huntington's disease. *Mol Ther* **16**, 947–56 (2008).
45. Zeng, Y. & Cullen, B. R. Structural requirements for pre-microRNA binding and nuclear export by Exportin 5. *Nucleic Acids Res* **32**, 4776–85 (2004).
46. Yang, N., Zhang, L. & Kazazian, H. H., Jr. L1 retrotransposon-mediated stable gene silencing. *Nucleic Acids Res* **33**, e57 (2005).
47. Klugmann, M. *et al.* A novel role of circadian transcription factor DBP in hippocampal plasticity. *Mol Cell Neurosci* **31**, 303–14 (2006).
48. Paxinos, G. & Franklin, K. B. J. *The Mouse Brain in Stereotaxic Coordinates* (Elsevier Academic Press, 2004).
49. Serrano, P. *et al.* PKMzeta maintains spatial, instrumental, and classically conditioned long-term memories. *PLoS Biol* **6**, 2698–706 (2008).
50. Ehninger, D. & Kempermann, G. Paradoxical effects of learning the Morris water maze on adult hippocampal neurogenesis in mice may be explained by a combination of stress and physical activity. *Genes Brain Behav* **5**, 29–39 (2006).

## Acknowledgments

We thank Paul Ruf, Gerhard Rimner, Simone Hoppe, Ulrike Bolz, and Gisela Eisenhardt for expert technical assistance and advice during this project, and Dr. Jeffrey A. Whitsett of the Cincinnati Children's Hospital Medical Center for kindly providing the GM-CSF knock-out mouse line.

## Author contributions

M. Krieger and AS designed the study. M. Krieger, MB, M. Klugmann, AD and AS wrote the manuscript. M. Krieger, MB, and SAK performed experiments. CP, M. Klugmann and GV provided research tools and contributed to data analysis. All authors reviewed the manuscript.

## Additional information

**Competing financial interests:** AS is inventor on patent applications claiming the use of GM-CSF for the treatment of neurological conditions.

**License:** This work is licensed under a Creative Commons Attribution-NonCommercial-NoDerivative Works 3.0 Unported License. To view a copy of this license, visit <http://creativecommons.org/licenses/by-nc-nd/3.0/>

**How to cite this article:** Krieger, M. *et al.* The hematopoietic cytokine granulocyte-macrophage colony stimulating factor is important for cognitive functions. *Sci. Rep.* **2**, 697; DOI:10.1038/srep00697 (2012).